



On the physics of ultrashort single-electron pulses for time-resolved microscopy and diffraction [☆]



Peter Baum

Max-Planck-Institute of Quantum Optics, and Ludwig-Maximilians-Universität München, Am Coulombwall 1, 85748 Garching, Germany

ARTICLE INFO

Article history:

Received 17 April 2013

In final form 14 June 2013

Available online 27 June 2013

Keywords:

4D diffraction

Attosecond science

Electron pulses

Ultrafast imaging

ABSTRACT

Pump–probe electron diffraction and ultrafast microscopy, based on laser excitation and probing with electrons, can provide a four-dimensional visualization of atomic motion in space and time. Electron pulses consisting of only single electrons have recently been used in order to avoid the deterioration of temporal resolution by Coulomb forces. Here it is discussed how one can define the pulse duration, the beam size and divergence, the transverse and longitudinal coherences, the energy spread and temporal dispersion, and the relation between bandwidth and shortest possible pulse duration, for single electrons and in practical context. Relations are provided on how to estimate these parameters from measurable quantities in a single-electron diffraction or microscopy experiment.

© 2013 The Author. Published by Elsevier B.V. All rights reserved.

1. Introduction

The course of a chemical reaction, or transformation in condensed matter, is ultimately defined by movements on the atomic scale. The primary steps involve the displacement of nuclei by picometers within times as short as femtoseconds. Electron densities also move on a picometer scale, but can do so within attoseconds. A full visualization of the reaction path, including the electronic and nuclear subsystems, hence requires a four-dimensional resolution of space and time, ideally in a direct way and without the need for much interpretation.

Capable techniques are pump–probe electron microscopy and diffraction [1–3]: laser pulses are used to impulsively initiate the course of the reaction, and electron pulses are used to provide a series of real-space images or diffraction patterns at increasing time delays, i.e. a stroboscopic sequence of structures. Electrons at 30–300 keV have a de Broglie wavelength of 2–7 pm, well sufficient for resolving atomic distances and their changes. With some efforts [3,4], the pulse durations can approach in the 100-femtosecond regime, which is sufficient for all but the very fastest atomic rearrangements found in photochemistry and phase transformations. Some proposals exist for approaching the attosecond regime of electron dynamics [5,7]. Ultrafast microscopy and diffraction share the pump probe principle but work in different

domains: microscopy provides direct images of femtosecond changes on nanometer scales, and diffraction can be used to resolve atomic motion with resolutions well below the bond length [8,9]. Electron diffraction was, for example, applied to photo-induced phase transformations in crystals [9–11], dissociations of molecules in the gas phase [12,13], melting processes [3,14], dynamics of surfaces [15,16], and many more. Ultrafast electron microscopy [17] was recently used to study, for example, the mechanical dynamics of DNA [18], the tomography of nanotubes [19], and many more [1].

Diffraction and microscopy with electrons notably discriminate from approaches with X-rays by a significantly shorter probing wavelength and by a much higher scattering cross section [20,21]. In comparison to free-electron lasers, the apparatuses are smaller in scale. There are, however, also drawbacks of using electrons: the high scattering cross section makes it necessary to fabricate ultrathin sections [22,23], or to use geometries with grazing incidence [24,25]. The small wavelength implies a rather low transverse coherence, which was only recently made sufficient to exceed biomolecular dimensions [23]. An additional problem is space charge: electrons repel each other, and the pulses lengthen in time during propagation from the point of generation to the sample. A trade-off must be made between the number of electrons per pulse and the desired temporal resolution [26–29]. Because a defined number of detected electrons is required for achieving atomic resolution of a complex molecule or crystal, this translates to a trade-off between the temporal resolution and the required size of the sample [29], or number of pump–probe cycles that the sample must be able to survive. There are two emerging regimes: single-shot and single-electron approaches. Single-shot

[☆] This is an open-access article distributed under the terms of the Creative Commons Attribution-NonCommercial-No Derivative Works License, which permits non-commercial use, distribution, and reproduction in any medium, provided the original author and source are credited.

E-mail address: peter.baum@lmu.de

diffraction [3,30,31] and microscopy [32,33] aim at producing a meaningful diffraction pattern of the sample with a single dense electron pulse at each pump–probe delay. This enables the study of irreversible processes, but requires the concentration of about 10^7 electrons to femtosecond duration while maintaining coherence and monochromaticity, a feat that is increasingly challenging as the dimensions of typical samples tend to decrease with complexity of the molecular structure. Reported techniques for achieving ultrafast resolution in the space charge regime include microwave cavities [31,34–37], chicanes [38], reflectrons [39], relativistic acceleration [40–43], energy-selective screens [44], streak cameras [45], or laser-plasma acceleration [46]. Depending on the amount of space charge, images can be significantly distorted in single-shot diffraction [47]. Nevertheless this regime seems inevitable for the study of irreversible processes such as melting.

Space-charge forces are ultimately avoided if the electron pulses consist of only one electron at a time. Individual electron wave packets do not repel themselves and no Coulomb forces distort the propagation of the pulses from the source to the sample. The perspective of this regime is to reach ultimate resolution down to attoseconds [5,6], useful for the study of electron dynamics [7]. Single-electron pulses were first applied in ultrafast electron microscopy [17,48] to avoid that spatial crossovers of the beam deteriorate the microscope's resolution; with pulses dense enough for one-time exposures this is only possible in the nanosecond regime [32,33]. Our use of single-electron pulses in a dedicated beamline has the purpose of pushing forward electron diffraction to, first, the ultimate regime of structural dynamics on a 10-fs scale, and later to the regime of electronic motions [7,49].

Probing structural dynamics by diffraction or microscopy requires accumulation of many single-electron detections for each pump probe delay. Typically, 10^7 – 10^9 incoming electrons are required, depending on the material's complexity. The measurement hence consists of a large number of pump/single-electron-probe cycles. On the screen, a meaningful image or diffraction pattern builds up sequentially from many single events, similar to Young's double-slit experiment. The pump–probe repetition rate should be as high as possible, but sufficiently low to allow the sample to relax back to the original state before the next excitation. In practice, the optimum is in the range of 0.1–5 MHz, and pulse energies of μJ are typically required. Femtosecond lasers are difficult to construct in that regime. We use a long-cavity oscillator [50] in combination with a pulse picker for adapting the repetition rate to the sample's relaxation dynamics. If necessary, the pulses can be shortened to the few-femtosecond regime [51], and optical parametric amplification can be used to match the excitation to sample's absorption spectrum [52]. At 0.1–1 MHz, a replacement of the sample between laser exposures becomes difficult, if not impossible. Accordingly, in advancing to novel resolution regimes with single electrons, we are accepting a restriction of our studies to processes with a certain degree of reversibility.

2. Single-electron pulses

The aim of this contribution is to provide an instructive picture of single-electron pulses, partially as a review and partially with new aspects not considered so far. Emphasis is on novel perspectives in the single-electron regime. First, it is summarized how ultrashort single-electron pulses at keV-scale energies can be generated (see Fig. 1); afterwards I discuss the essential characteristics of the resulting pulses (see Fig. 2).

In photoelectric surface sources (Fig. 1a), ultraviolet laser pulses impinge on a metal film (red). At photon energies above the work function, photoelectrons are generated and accelerated to keV-range energies with a static field between the emitter and an anode. The blue arrows illustrate the random emissions of individual electrons, having distributions of origins and velocities as a consequence of the statistical nature of photoelectric emission from realistic metals [4]. An alternative approach are needle sources [53–56], depicted in Fig. 1b. Femtosecond laser pulses are focused onto a sharp needle of metal with a tip radius of down to nanometers. Advantages of such sources are the extreme localization of the emission area and the enhancement of the acceleration field by near fields at the tip. A disadvantage is the strongly inhomogeneous distribution of initial trajectories, causing a large divergence and temporal distortions [56]. A third type of electron source, depicted in Fig. 1c, is based on the photoionization of ultracold gases [29,57,58]. Such sources have a rather large size determined by the ionized volume, but an extremely low temperature and energy spread [29,58]. However, the repetition rate is restricted by the time it takes to cool down the gas cloud after photoemission. Femtosecond pulses have not yet been generated from cold gases; likely the pulse duration will be limited by the traveling time of the ionizing laser through the gas cloud. In all schemes, an electrostatic or magnetic lens system is needed in order to collimate or refocus the beam to the sample location or screen [28]. Ideally this imaging is 'isochronic' [59], i.e. providing the same timing for different trajectories through the system.

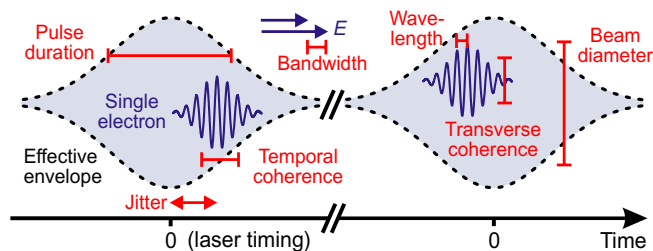


Fig. 2. Single-electron pulses and essential parameters. Depicted are two single-electron emissions, triggered by femtosecond laser pulses, forming a pulse train useful for pump–probe studies via diffraction or microscopy. Marked are the pulse duration, bandwidth, de Broglie wavelength, temporal and transverse coherences, jitter, beam diameter, and the effective envelope of the electron pulse shape.

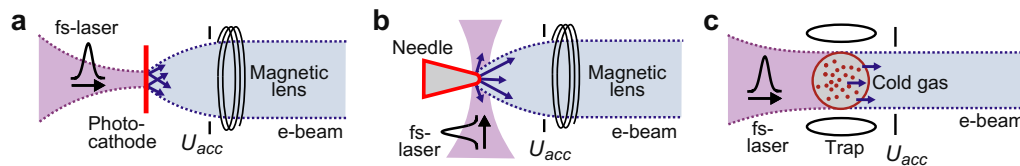


Fig. 1. Three experimental approaches suitable for generation of ultrashort single-electron pulses. (a) Femtosecond photoelectric emission from a metal layer (red) produces electrons with momentum spread (blue arrows), forming a beam (light blue) in the acceleration field U_{acc} . (b) Laser excitation of a nanometer-sized needle produces extremely well localized electrons, albeit with a larger momentum spread (blue arrows). (c) Photo-ionization of an ultracold gas (red) can produce electron pulses with extremely low divergence (blue arrows), albeit with a larger source size than in the other schemes. For details of single-electron operation and references see Section 2. (For interpretation of the references to color in this figure legend, the reader is referred to the web version of this article.)

In all three types of laser-based sources, single-electron pulses are generated if the optical intensity is attenuated sufficiently, for example in the flat emitters to about picojoules of incident energy per pulse. At such conditions, electrons are generated in a statistical way and less than one electron per pulse is generated on average; i.e. the probability of having two electrons in one pulse can be made very small. For example, if electron emission is described by shot noise with a Poisson statistics, a beam with 0.5 electrons per pulse has less than 10% of pulses having two or more electrons. Space charge is absent in single-electron pulses in a fundamental way, because a one-electron wave packet does not show internal Coulomb repulsion within itself.

Propagation is solely determined by the initial conditions of the electron wave packet and the distributions from pulse to pulse. Accordingly, there are two types of parameters in a train of single electrons such as used in pump–probe experiments: those describing the single electrons as quantum objects, and those related to the statistics of the many pulses producing a diffraction pattern or image. An attempt to depict this instructively is shown in Fig. 2. Topic of the following sections is how to estimate the depicted parameters, and what implications they have for applications. Briefly, the central energy E_0 determines the de Broglie wavelength λ_0 , essential for atomic-scale resolution, and the central speed v_0 , essential for how much time the pulses spend in free space before the sample (see section 3). The bandwidth ΔE is a consequence of the photoemission process on the femtosecond scale and causes temporal broadening even without space charge (see section 4). The beam radius σ_\perp and the transverse momentum spread σ_{p_\perp} originate from the limited emittance at the source and are affected by the imaging system (see section 5). The transverse coherence ξ_\perp determines the ability of single electrons to diffract from atoms that are far apart; in the experiment this is a decisive factor for the spatial resolution of complex materials (see section 6). The longitudinal coherence ξ_\parallel determines the ability of electrons to interfere with themselves in time; this becomes important in the experiment if temporal pulse compression is applied (see section 7). Finally, in section 8, I discuss some limitations for the minimally achievable pulse duration in dependence of the bandwidth and the temporal coherence, in analogy to the concept of ‘Fourier limit’ that is commonly used in femtosecond and attosecond optics.

3. Energy, bandwidth, pulse duration

A useful range of energy for applications of electron pulses in microscopy is $E_0 = 30\text{--}300$ keV, in diffraction up to MeV. With the electron mass m_e and the speed of light c , the momentum p_\parallel is $p_\parallel = \frac{1}{c} \sqrt{E_0^2 + 2E_0(m_e c^2)}$. The de Broglie wavelength is $\lambda_0 = h/p_\parallel$. For 30–300 keV, it is about 2–7 pm, which is around ten to a hundred times shorter than atomic distances and hence a good range for diffraction at convenient angles. Many Bragg orders can typically be observed simultaneously [9,23]. Lower electron energies have the advantage of reduced radiation damage, but maintaining a good spatial and temporal resolution in an electron microscope or diffraction beamline is more challenging. Higher energies in the MeV range [40–43] provide relaxed restrictions on the sample's thickness and alleviate the effects of space charge, but the too small diffraction angles and difficulties with magnetic imaging make the experiment more complicated.

The bandwidth ΔE in the single-electron regime is determined by the physics of photoemission in connection with the bandwidth of the femtosecond laser pulses [4]. In the following, we use ΔE defined by the full width at half maximum and $\sigma_E \approx \Delta E / \sqrt{8 \ln 2}$ as the standard deviation for Gaussian and similar distributions. At

crystalline surfaces of good quality, photoemission can promote the initial electronic states in the material to vacuum preserving bandwidth, localization and momentum [60]. In contrast, photocathodes made of realistic metal surfaces have distributions of facets and are rough [61], hence photoemission is inhomogeneous and most of the phase space that is energetically available seems to be occupied [4,61,62], if crystal momentum is not conserved [63]. In the single-electron regime, a match between the laser's photon energy and the cathode material's work function is therefore useful to reduce the electron pulses' velocity spreads in longitudinal and transverse directions [4]. For practical flat femtosecond cathodes, an effective $\Delta E \approx 0.1$ eV [64] and $\Delta E = 0.08\text{--}0.3$ eV [4] were determined experimentally. Tip emitters should have similar values [56]. After acceleration to 30–300 keV, the degree of monochromaticity, $\Delta E/E$, is in the range of 10^{-5} to 10^{-6} . This is almost as good as in state-of-the-art conventional electron microscopes, but with femtosecond pulses.

Quite often the question comes up of how to correctly think of the pulse duration in the single-electron regime. In Fig. 2 it is illustrated as the width of the statistical envelope of electrons, in relation to a recurring time-zero determined by the timing of the laser pulses. This depiction is made with practical experiments in mind, where many single-electron detections, about 10^7 or more, are required to form an image or diffraction pattern with enough information about atomic positions. As discussed above, the pump–probe experiment is a sequence of many pump/single-electron detection cycles. Each single electron might be localized in time, resembling a point charge, but decisive for the pulse duration and resolution in the experiment is the distribution of arrival times of the electrons at the sample, with respect to the laser's timing. The pulse duration of single-electron pulses is therefore here defined by the full width at half maximum of the envelope of arrival times at a given position in space, in relation to the laser timing, like depicted in Fig. 2; see also Ref. [4]. This is in analogy to the definitions of the spatial parameters such as beam diameter and divergence, concepts that only make sense in the single-electron regime as averages over many single-electron emissions.

Only a few techniques exist for directly measuring the duration of ultrashort electron pulses of low or single-electron density. The approach used in synchrotrons, coherent transition radiation, cannot practically be applied in the single-electron regime, because the intensity of emitted radiation scales about quadratically with the number of electrons in the pulse. Another approach is cross-correlation of electrons with the ponderomotive force of laser pulses [65], but the temporal resolution in that scheme is limited by the laser pulse duration and the time the electrons need to pass through the laser focus. Pulse durations of 300–500 fs were measured in that way [31,35]. Another idea is to streak Auger electrons in a few-cycle laser field [66]; this scheme potentially offers attosecond resolution but suffers from the very low rate of Auger processes in the single-electron regime. An energy filter in connection with a microwave cavity for pulse compression [37] could provide the pulse durations if the laser-microwave jitter was known to be low enough. In practice, an upper limit for the electron pulse duration is also given by the fastest measured dynamics [9,67].

4. Dispersion

Vacuum is dispersive for non-relativistic electrons, i.e. electrons with higher energy travel faster than those with lower energy. The bandwidth at the source hence causes a temporal broadening of the pulses during propagation. In the experiments applying flat photoelectron emitters, one can distinguish two contributions, one from the acceleration region between cathode and anode, and one from propagation in free space afterwards. For flat

cathodes with constant electrostatic acceleration the literature offers different formulas, which share the same proportionalities but have differing pre-factors, resulting from the assumptions made on the three-dimensional distribution of initial velocities after photo-emission; see section 11 in Ref. [37]. Assuming an isotropic emission into a half-sphere and a constant acceleration field U_{acc} , we obtain $\tau_{\text{acc}} \approx \sqrt[4]{2\sqrt{m_e \Delta E} / (eU_{\text{acc}})}$ [4]. In free space, after propagation at final speed for a distance L , one obtains a lengthening of $\tau_{\text{free}} \approx \frac{L}{v(E_0)} - \frac{L}{v(E_0 + \Delta E_0)}$, with the velocity $v(E)$. For example, our diffraction beamline (without the microwave compressor) at good conditions has $U_{\text{acc}} = 8 \text{ kV/mm}$, $E_0 = 60 \text{ keV}$, $\Delta E \approx 0.2 \text{ eV}$ or better [4], and the distance between source and sample is $L \approx 50 \text{ cm}$. For these values, one obtains $\tau_{\text{acc}} \approx 180 \text{ fs}$ and $\tau_{\text{free}} \approx 5 \text{ fs}$. The temporal distortions of the magnetic lens amount to about 30 fs [59]. The final pulse duration is given by convolution of all these broadening mechanisms. Largest is the contribution of the acceleration region, which we already constructed in a way close to technological limitations [4,23]. Tip sources suffer from the same mechanism of dispersion, with stronger acceleration but less monochromaticity in forward direction; 200-fs pulses can be expected at a sample [56]. Achieving electron pulse durations in the few-fs or eventually sub-fs regime hence requires additional approaches such as microwaves or optical gratings; see section 8.

5. Beam size and divergence

Multiple single-electron emissions produce a beam with a diameter and divergence. An electron beam is partially incoherent, i.e. the divergence in a waist is not a priori related to the waist size, like it would be the case for Gaussian laser beams. The spatial characteristics of an electron beam are described (to first order) by the beam radius σ_{\perp} and the distribution of transverse momentum $\sigma_{p_{\perp}}$. The emittance at a waist, $\varepsilon_{\perp} = \frac{\sigma_{\perp} \sigma_{p_{\perp}}}{m_e c}$ [29], is conserved during propagation in linear elements; hence, beam size can be traded versus divergence and vice versa. Emittance is related to coherence [29]; see section 6 below. Initially, a beam's emittance is determined by the processes at the electron source, specifically by the size of the emitter and its energy spread. In flat photocathodes, the emission size is determined by the optical focus of the laser, and can be made as small as a few μm in the absence of space charge [23]. The lateral velocity spread of single electrons from flat surfaces is low, about 140 km/s [4,23]. A temperature can be assigned using $\sigma_{p_{\perp}} = \sqrt{m_e k_B T}$ [29]. In our beamline we have about 1300 K at the source and about 1–3 K in the collimated beam, depending on size. The emittance is $\varepsilon_{\perp} \approx 3 \text{ nm}$ (0.003 mm mrad). In tip emitters, the effective source size can be much smaller, in the nanometer range, but the divergence is larger and mostly determined by inhomogeneous near fields of the acceleration potential [56]. Assuming a tip diameter of 50 nm and a full divergence of $\pm 5^\circ$, the emittance is on the scale of 1 nm (0.001 mm mrad), but it still needs to be demonstrated that the temporal distortions induced by the local field enhancement can be compensated for, in order to deliver femtosecond single-electron pulses to the location of a sample.

Apertures can be used to spatially filter the beam, improving the emittance at cost of flux. Such apertures are frequently used in conventional electron microscopes, where many more electrons per second are initially generated than effectively arrive at the sample. This, however, is problematic in time-resolved experiments. In order to obtain one electron per pulse at the sample, desirable to avoid unnecessary excitations by the pump laser, more have to be generated before the apertures. This possibly introduces space charge and broadening in the region before the aperture. The lengthening in time before the aperture may be small, but space charge also induces a significant growth of energy spread, which

causes a continuously progressing dispersion even after selection of single electrons by the aperture. In addition, magnetic lenses are prone to chromatic aberrations. In our beamline, we hence refrain from using any spatial filters and instead try to minimize the primary emittance at the source, by reducing size and divergence [4,23]. Every single electron generated at the source arrives at the sample.

Measurement of source size and divergence can be obtained by a B-field scan, i.e. a recording of beam diameters on a screen in dependence of the strength of a magnetic lens [23]. For the source in our experiment, we obtain a radius of $\sigma_{\perp} \approx 3 \mu\text{m}$ and a transverse velocity spread of $\sigma_{p_{\perp}}/m_e \approx 140 \text{ km/s}$ in this way. This is sufficient for single-electron diffraction from complex organic molecules approaching biomolecular sizes [23].

6. Transverse coherence

The ability of electrons to resolve atoms and their distances, for example in diffraction or by related contrast mechanisms in microscopy, is a result of their behavior as de Broglie waves. The transverse coherence of an electron beam denotes the ability to produce interference from scatterers that are far apart. Coherence hence determines the ability to resolve complex structures. In order to obtain a full and direct resolution of all atoms and their motion, the molecular nanostructure or unit cell in a crystal should be entirely covered by a coherent electron wave, in order to not lose important information. Many molecules with relevance to chemistry and biology have sizes of tens of nanometers; this determines the magnitude of coherence that the electron pulses should have.

A comprehensive description of coherence in electron microscopy involves the coherence transfer and correlation functions [68]. However, a characteristic value ξ_{\perp} for the transverse coherence length can also be obtained by simpler means. For the case of a beam passing through an aperture, such as in electron microscopes, one can apply the Cittert–Zernike theorem, stating that an incoherently, homogeneously illuminated, disk-like aperture becomes partially coherent at a distance [69]. Applying an 88%-criterion for the visibility of interference fringes, and using the aperture's radius R and the distance L , one obtains $\xi_{\perp} = \lambda_0 L / (2R)$ [17,70]. Sometimes these types of definitions include an additional factor of π [68,70,71]. Without the π , and if one approximates the geometric half-angle $\theta = R/L$ with $\theta \approx \sigma_{p_{\perp}}/p_{\parallel}$, one obtains $\xi_{\perp} \approx h/\sigma_{p_{\perp}}$.

Alternatively, the transverse coherence length ξ_{\perp} at a beam waist can be defined by $\xi_{\perp} = \lambda / (2\pi\sigma_{\theta})$ [72], where σ_{θ} is the uncorrelated angular spread $\sigma_{\theta} = \sigma_{p_{\perp}}/p_{\parallel}$, i.e. the half-angle divergence. Written in terms of transverse velocity spread, one obtains $\xi_{\perp} = h/\sigma_{p_{\perp}}$. This equation, derived from optical visibilities, is a broadly accepted definition in the field of ultrafast electron diffraction [3,4,23,29,72]. Note that ξ_{\perp} is a full width, i.e. an entirely coherent beam has $\xi_{\perp} = 2\sigma_{\perp}$. The coherence cannot be larger than the beam diameter.

Here is another approach, novel to my knowledge, based on an application of the uncertainty relation. In any beam, the lateral momentum spread $\sigma_{p_{\perp}}$ is easily measured, for example $\sigma_{p_{\perp}}/m_e \approx 6 \text{ km/s}$ in our beamline at the sample [23]. Using the uncertainty relation, that well-defined, small value for $\sigma_{p_{\perp}}$ imposes a lower limit on the radius $\sigma_{\psi_{\perp}}$ that the wave function describing the electrons must minimally have: $\sigma_{p_{\perp}} \sigma_{\psi_{\perp}} \geq h/2$. Hence the diameter of the delocalized wave packet, twice the radius, obeys $2\sigma_{\psi_{\perp}} \geq h/\sigma_{p_{\perp}}$. Each single electron can interfere with itself. If one assumes that the wave function's diameter determines the transverse coherence, i.e. $\xi_{\perp} = 2\sigma_{\psi_{\perp}}$, one can derive $\xi_{\perp} \geq h/\sigma_{p_{\perp}}$. Interestingly, this result is similar to the conventional definitions, despite the allowedly simple derivation here. The uncertainty

Table 1

Comparison of different approaches for estimating a value for transverse coherence in an electron beam.

Approach	Cittert–Zernike theorem	Definition in beams	uncertainty relation
Result	$\xi_{\perp} = \lambda_0 \frac{1}{2R}$, $\xi_{\perp} \approx h/\sigma_{p_{\perp}}$	$\xi_{\perp} = h/\sigma_{p_{\perp}}$	$\xi_{\perp} \geq h/\sigma_{p_{\perp}}$
Refs.	[68–70]	[29,72]	(this work)

relation can replace the choice of a visibility criterion or selection of a particular geometry. Also, the uncertainty approach can describe the coherence directly at a source, before acceleration and formation of a practical beam. Table 1 summarizes the different approaches and their results.

In diffraction experiments, converging or diverging beams are sometimes used at the sample [23,28]. Magnification of the beam also magnifies the coherence [73,23], because the global degree of coherence $\beta_{\perp} = \xi_{\perp}/(2\sigma_{\perp})$ is conserved, i.e. the ratio of coherence length and beam diameter stays constant [73,23]. Note that β_{\perp} is here defined such that it becomes one for the fully coherent beam. In an experiment, it is in principle possible to improve the coherence arbitrarily by sufficiently magnifying the beam, but this is only practical if large enough samples are available. This is hardly the case for complex materials. The size of the diffraction sample limits the maximally useful beam diameter, and the coherence in that beam determines the sharpness of the diffraction features and ability to track all atomic positions. Practically important for diffraction experiments is therefore the magnitude of the transverse coherence in relation to the size of the specimen under investigation [29].

For multi-electron beams, the transverse coherence was estimated 2–3 nm for beams with $\sigma_{\perp} \approx 150$ –200 μm [28,72], and for single electrons it was recently shown to reach 20 nm for a beam with $\sigma_{\perp} < 100 \mu\text{m}$ [23]. The latter result ($\beta_{\perp} \approx 10^{-4}$) is made possible by focusing the photoemission laser tightly onto the photocathode, minimizing the area of electron emission; in addition, the divergence is low in the absence of space charge. Hence, time-resolved and coherent diffraction from samples with unit cell sizes up to biomolecular dimensions is conceivable with single-electron pulses, if samples with radii of about 100 μm are available. It will be interesting to see whether femtosecond needle sources or cold gas emitters can provide an improvement here, in practice [56,58].

7. Temporal coherence

The coherence time ξ_t and the longitudinal coherence length $\xi_{\parallel} = v_0 \xi_t$ describe the ability of electron waves to interfere in time and in propagation direction. While this is almost irrelevant for diffraction [74], temporal coherence becomes important if electron pulses are compressed in time or if energies are measured in a time-resolved experiment. In order to be similar to the spatial case, it is here chosen that ξ_{\parallel} shall denote a full length (2σ), meaning that the fully coherent pulse has $\xi_{\parallel} = 2\sigma_{\parallel}$; the longitudinal coherence cannot be larger than the longitudinal extent of the pulse. The coherence time ξ_t is then in relation to the pulse duration, i.e. the pulses are maximally coherent if ξ_t equals the full pulse duration ($2\sigma_t$). Like for the spatial case, one can define a global degree of temporal coherence, $\beta_t = \xi_t/(2\sigma_t)$, such that the fully coherent pulse has $\beta_t = 1$. In analogy to the global degree of coherence in the spatial domain [73], the global degree of temporal coherence is conserved in elements affecting the beam linearly in time.

In order to obtain an estimation for ξ_t and ξ_{\parallel} , one can apply the uncertainty relation in a similar way as before. The energy spread σ_E in the beam is well-defined and low; for example

$\sigma_E \approx \Delta E/\sqrt{8 \ln 2} \approx 0.085 \text{ eV}$ or better [4]. Applying the uncertainty relation in the time-energy domain [75], this well-defined energy spread imposes a lower limit on the duration σ_{ψ_t} that the wave function must have: $\sigma_E \sigma_{\psi_t} \geq \hbar/2$. Each electron can interfere with itself. If one defines the coherence time (in analogy to the spatial definition) as twice the σ -value of the wave function's longitudinal extent, i.e. $\xi_t = 2\sigma_{\psi_t}$, one can derive $\xi_t \geq \hbar/\sigma_E$ and $\xi_{\parallel} \geq v_{\parallel} \hbar/\sigma_E$.

Under good conditions, the single-electron pulses in our beam-line have $E_0 \approx 60 \text{ keV}$, $\Delta E \approx 0.2 \text{ eV}$, $\sigma_E \approx 0.085 \text{ eV}$ and $v_{\parallel} \approx 0.45c$. These values predict a longitudinal coherence length of $\xi_{\parallel} \approx 1 \mu\text{m}$ and a coherence time of $\xi_t \approx 7.8 \text{ fs}$ or more. Hence the single-electron wave packets consist of more than 10^5 coherent cycles of the de Broglie wave. Pulses with $\Delta E = 0.2 \text{ eV}$ have a full-width-at-half-maximum pulse duration of about 150 fs when leaving an optimized electron source [4], i.e. $\sigma_t \approx \frac{150 \text{ fs}}{\sqrt{8 \ln 2}} \approx 70 \text{ fs}$. With the temporal coherence derived above, $\xi_t \approx 7.8 \text{ fs}$, the global degree of temporal coherence is $\beta_t = \xi_t/(2\sigma_t) \approx 0.06$. This is a lower limit, because the 150-fs pulses have some chirp (see section 4) and could be shorter while having the same energy spread, for example in sources with higher acceleration fields. With a coherence time of more than 6% of the pulse duration, our pulses are not too far from being fully coherent in time. Multi-electron pulses are much less coherent in time, because the energy spread can easily exceed hundreds of eV, as a consequence of the longitudinal space-charge forces.

Interestingly, the temporal coherence of single-electron pulses exceeds about two or three times the duration of an optical cycle in a typical laser pulse, for example 2.7 fs at 800 nm. If a laser field is used to increase or decrease the energy of an electron pulse, the same final energy may be reached for two or more different cycles of the laser field, making it possible that constructive or destructive interference appears in the electron's energy spectrum. Such interferences were predicted for streaking experiments of Auger processes [66] and experimentally recorded in photon-induced near-field electron microscopy [67], both in the single-electron regime. The derivations made in this section indicate that the width of the measured energy maxima in such experiments could be a direct measure of temporal coherence in the electron pulses.

8. Limits of pulse compression

As outlined in Section 4, it is largely impossible to generate few-femtosecond or attosecond electron pulses directly with a static electron source; in particular, electron pulses cannot be shorter than the duration of the generating laser pulses. For reaching into the attosecond regime, there are concepts for time-dependent compression elements providing acceleration and deceleration of parts of the single-electron pulses. One idea is based on longitudinal fields in a microwave cavity [5,37], and another idea applies the longitudinal ponderomotive forces in optical gratings [6,7]. Both schemes can be viewed as 'temporal lenses' [76], i.e. leading parts of the electron pulse are decelerated and trailing parts are accelerated. This generates a tilted phase space in the time-energy domain, with leading electrons having less energy than the ones behind. Next, the dispersion of vacuum leads to a compression at some point in space, where the faster electrons have caught up with the slower ones. Assuming that phase space volume is conserved, which is the case for forces linear in time, the pulses hence shorten in duration at cost of an extent in energy spread; compare also Fig. 2 of Ref. [37]. The more gain in energy bandwidth, the shorter become the pulses. A certain energy spread, however, must not be exceeded in diffraction and microscopy, if not to distort the images by distributions of de Broglie wavelengths or chromatic aberrations in the lens system.

In order to estimate the shortest possible pulse duration for an experimentally given energy bandwidth after a temporal compression element, we consider the longitudinal emittance ε_{\parallel} in the time domain: $\varepsilon_{\parallel} = \sigma_t \sigma_E / (m_e c)$ [29]. This definition holds for a longitudinal beam waist [29], i.e. at a position where the bunch has no chirp. ε_{\parallel} is conserved in linear temporal elements. For example, the time-dependent field in a microwave cavity oscillates with periods that are much longer than the time it takes the electron to pass through [37]; hence the cavity compressor is a good example of a linear temporal lens. To some extent the ponderomotive scheme can also be treated linearly, as a weak approximation and lower limit. Assuming conservation of phase space volume, the compression from initial to final pulse durations obeys $\sigma_t^{final} \sigma_E^{final} = \sigma_t \sigma_E$ in an imaging from one temporal focus to another. This allows deriving a simple relation for the minimally achievable pulse duration σ_t^{final} after a compressor. Using $\beta_t = \xi_t / (2\sigma_t) = \hbar / (2\sigma_t \sigma_E)$, one obtains $\sigma_t^{final} = \hbar / (2\beta_t \sigma_E^{final})$. Written for full-width-at-half-maximum values ΔE^{final} and Δt^{final} , one obtains $\Delta t^{final} = (8 \ln 2) \hbar / (2\beta_t \Delta E^{final})$.

This relation is an electron-optical analogon to the time-bandwidth product and Fourier limit in laser optics, where the limit of pulse duration is determined by the spectrum's bandwidth. In contrast to lasers, however, the limited temporal coherence in electron pulses further lengthens the achievable pulse duration above what could be expected from just the total energy bandwidth. Imperfection of temporal coherence restricts the ability to focus in time. This is analogous to the spatial dimensions, where incoherence restricts the ability to focus the beam tightly.

The influence of temporal coherence to pulse compression can be illustrated at the example of the microwave cavity compressor. Leading electrons are decelerated and trailing ones are accelerated, producing a total bandwidth σ_E^{final} over the pulse duration $\sigma_t \approx 70$ fs. However, the single-electron wave packets of (full) duration $\xi_t \approx 7.8$ fs only gain a fraction β_t of that energy spread, each individually. Via the time-energy uncertainty relation [75], this smaller bandwidth $\beta_t \sigma_E^{final}$ and not the total bandwidth over all electrons determines the minimally achievable pulse duration; the pulse cannot be shorter than each single-electron wave function. In the experiment, if the shortest electron pulses are sought for, it is therefore important to maximize the temporal coherence of the single-electron source.

One can now evaluate the general potential of temporal lenses for achieving attosecond pulse durations in practice. Assuming that 100-attosecond pulses (full width at half maximum) are to be generated at a central energy of 60 keV, and using the temporal degree of coherence of 6% as derived above, one obtains that the spectrum after the compression element must be broader than 300 eV (full width at half maximum). For 10-attosecond pulses, it is 3 keV. These bandwidths seem large, but are still useful for diffraction, because the spread of de Broglie wavelength is only a few percent. On the other hand, high-resolution electron microscopy will be at least difficult if not impossible at such energy spreads, because the aberrations in the lens systems become severe.

At 60 keV, it takes about 7 attoseconds to pass a unit cell of 1 nm. Pulses shorter than that may not any more diffract in the usual way, but in the regime of hundreds of attoseconds, relevant for the electron dynamics of bound states, diffraction seems to behave as expected [7,49]. However, energy exchange between the incoming probe wave and the moving electron density under investigation should be avoided if not to obstruct the obtained information [77]. Fortunately, electron–electron exchange interaction seems negligible in single-electron diffraction at energies above a few keV [49]. A pump–probe approach, probably with few-cycle laser fields for inducing the motion of charge densities and with time-resolved single-electron diffraction of shortest duration, seems a viable perspective for imaging electronic processes on atomic scales in both space and time.

Table 2

Table 2 Summary of the parameters discussed in the text, and measured or expected values in a single-electron diffraction beamline [4,23] with microwave compression cavity [37]. In practice, not all values may be that good at the same time.

Parameter	Meaning	Value in our single-electron beamline
E_0	central energy	up to 60 keV
ΔE	energy spread (full width at half maximum)	0.2 eV (down to 0.08 eV)
σ_E	energy spread (sigma)	0.085 eV
$\Delta E/E_0$	monochromaticity	10^{-5} – 10^{-6}
U_{acc}	acceleration field	up to 8 kV/mm
λ_0	De Broglie wavelength	5 pm
v_0	central electron speed	0.45c
p_{\parallel}	central longitudinal momentum	$0.5c m_e$
Δt	pulse duration (full width at half maximum)	100–400 fs
σ_t	pulse duration (sigma)	40–170 fs
ξ_t	temporal coherence	7.8 fs
ξ_{\parallel}	longitudinal coherence length	1 μ m
ε_{\perp}	emittance	3 nm (0.003 mm mrad)
ε_{\parallel}	longitudinal emittance	4 pm
σ_{\perp}	beam radius (sigma)	2.7 μ m at the source
$\sigma_{p_{\perp}}$	transverse momentum spread (sigma)	(140 km/s) m_e at the source
ξ_{\perp}	transverse coherence	20 nm for a 100- μ m spot
β_{\perp}	global degree of coherence	10^{-4}
β_t	global degree of temporal coherence	0.06
ΔE^{final}	bandwidth after microwave cavity	180 eV
Δt^{final}	compressed pulse duration (limit)	0.3 fs (plus microwave jitter)

9. Remarks and outlook

The parameters depicted in Fig. 2 can certainly provide only a quite simplified picture of single-electron pulses. Not considered are various linear and nonlinear deformations in spatiotemporal phase space, quantum descriptions of coherence, and relativistic effects. Nevertheless, Fig. 2 and the above discussions should be helpful for future applications of single electrons in ultrafast diffraction, microscopy, imaging and spectroscopy. Table 2 provides a list of the parameters discussed in the text, and the values they can have in single-electron diffraction at good conditions; for details see Refs. [4,23,37,59].

In optics, it took several decades to shorten the pulses into the femtosecond, recently attosecond regimes [78]. Light fields can be fully controlled [79] and measured by attosecond streaking [80]. On this technological route, time-resolved spectroscopy advanced along, always revealing novel effects at each available resolution [81], today in the attosecond domain [82,83]. Single-electron pulses in free space have potential to catch up, and overtake. Pulse durations are essentially unlimited and the de Broglie wavelength is convenient for atomic-scale imaging and diffraction. Conceivably, single-electron pulses may become a valuable alternative to light and X-rays for investigations of physics and chemistry at the ultimately shortest scales of time.

Acknowledgments

I thank F. Krausz, F. O. Kirchner and S. Lahme for carefully reading the manuscript and valuable corrections, and O. J. Luiten for helpful discussions about coherence and the uncertainty relation. This research is supported by F. Krausz and funded by the European Research Council ('4D imaging'), the Munich-Centre of Advanced Photonics, and the Rudolf-Kaiser Foundation.

References

- [1] D.J. Flannigan, A.H. Zewail, *Acc. Chem. Res.* 45 (2012) 1828.
- [2] A.H. Zewail, *Annu. Rev. Phys. Chem.* 57 (2006) 65.
- [3] G. Sciaini, R.J.D. Miller, *Rep. Prog. Phys.* 74 (2011) 096101.
- [4] M. Aidelburger, F.O. Kirchner, F. Krausz, P. Baum, *Proc. Natl. Acad. Sci. U.S.A.* 107 (2010) 19714.
- [5] L. Veisz, G. Kurkin, K. Chernov, V. Tarnetsky, A. Apolonski, F. Krausz, E. Fill, *New J. Phys.* 9 (2007) 451.
- [6] P. Baum, A.H. Zewail, *Proc. Natl. Acad. Sci. U.S.A.* 104 (2007) 18409.
- [7] P. Baum, A.H. Zewail, *Chem. Phys.* 366 (2009) 2.
- [8] F. Carbone, P. Baum, P. Rudolf, A.H. Zewail, *Phys. Rev. Lett.* 100 (2008) 035501.
- [9] P. Baum, D.-S. Yang, A.H. Zewail, *Science* 318 (2007) 788.
- [10] N. Gedik, D.-S. Yang, G. Logvenov, I. Bozovic, A.H. Zewail, *Science* 316 (2007) 425.
- [11] M. Eichberger, H. Schäfer, M. Krumova, M. Beyer, J. Demsar, H. Berger, G. Moriena, G. Sciaini, R.J.D. Miller, *Nature* 468 (2010) 799.
- [12] H. Ihee, V.A. Lobastov, U.M. Gomez, B.M. Goodson, R. Srinivasan, C.-Y. Ruan, A.H. Zewail, *Science* 291 (2001) 458.
- [13] C.J. Hensley, J. Yang, M. Centurion, *Phys. Rev. Lett.* 109 (2012) 133202.
- [14] R. Ernstorfer, M. Harb, C.T. Hebeisen, G. Sciaini, T. Dartigalongue, R.J.D. Miller, *Science* 232 (2009) 1033.
- [15] D.-S. Yang, O.F. Mohammed, A.H. Zewail, *Proc. Natl. Acad. Sci. U. S. A.* 107 (2010) 14993.
- [16] W. Liang, S. Schäfer, A.H. Zewail, *Chem. Phys. Lett.* 542 (2012) 1.
- [17] A.H. Zewail, *Science* 328 (2010) 187.
- [18] U.J. Lorenz, Ahmed H. Zewail, *Proc. Natl. Acad. Sci. U.S.A.* 110 (2013) 2822.
- [19] O.-H. Kwon, Ahmed H. Zewail, *Science* 328 (2012) 1668.
- [20] M. Chergui, A.H. Zewail, *Chem. Phys. Chem.* 10 (2009) 28.
- [21] F. Carbone, P. Musumeci, O.J. Luiten, C. Hebert, *Chem. Phys.* 392 (2012) 1.
- [22] M. Eichberger, M. Krumova, H. Berger, J. Demsar, *Ultramicroscopy* 127 (2013) 9.
- [23] F.O. Kirchner, S. Lahme, F. Krausz, P. Baum, *New J. Phys.* 15 (2013) 063021.
- [24] P. Baum, A.H. Zewail, *Proc. Natl. Acad. Sci. U.S.A.* 134 (2006) 16105.
- [25] D. Kreier, P. Baum, *Opt. Lett.* 37 (2012) 2373.
- [26] B.J. Siwick, J.R. Dwyer, R.E. Jordan, R.J.D. Miller, *J. Appl. Phys.* 92 (2002) 1643.
- [27] S. Collin, M. Merano, M. Gatri, S. Sonderegger, P. Renucci, J.-D. Ganière, B. Deveaud, *J. Appl. Phys.* 98 (2005) 094910.
- [28] A. Gahlmann, S.T. Park, A.H. Zewail, *Phys. Chem. Chem. Phys.* 10 (2008) 2894.
- [29] S.B. van der Geer, M.J. de Loos, E.J.D. Vredenburg, O.J. Luiten, *Microsc. Microanal.* 15 (2009) 282.
- [30] R.K. Li, P. Musumeci, H.A. Bender, N.S. Wilcox, M. Wu, *J. Appl. Phys.* 110 (2011) 074512.
- [31] M. Gao, H. Jean-Ruel, R.R. Cooney, J. Stampe, M. de Jong, M. Harb, G. Sciaini, G. Moriena, R.J.D. Miller, *Opt. Express* 20 (2012) 12048.
- [32] B.W. Reed, M.R. Armstrong, N.D. Browning, G.H. Campbell, J.E. Evans, T. LaGrange, D.J. Masiel, *Microsc. Microanal.* 15 (2009) 272.
- [33] O.-H. Kwon, B. Barwick, H.S. Park, J.S. Baskin, A.H. Zewail, *Proc. Natl. Acad. Sci. U.S.A.* 105 (2008) 8519.
- [34] T. van Oudheusden, P.L.E.M. Pasmans, S.B. van der Geer, M.J. de Loos, M.J. van der Wiel, O.J. Luiten, *Phys. Rev. Lett.* 105 (2010) 264801.
- [35] R.P. Chatelain, V.R. Morrison, C. Godbout, B.J. Siwick, *Appl. Phys. Lett.* 101 (2012) 081901.
- [36] G.H. Kassier, N. Erasmus, K. Haupt, I. Boshoff, R. Siegmund, S.M.M. Coelho, H. Schwoerer, *Appl. Phys. B* 109 (2012) 249.
- [37] A. Gliserin, A. Apolonski, F. Krausz, P. Baum, *New J. Phys.* 14 (2012) 073055.
- [38] S. Tokita, M. Hashida, S. Inoue, T. Nishoji, K. Otani, S. Sakabe, *Phys. Rev. Lett.* 105 (2010) 215004.
- [39] G.H. Kassier, K. Haupt, N. Erasmus, E.G. Rohwer, H. Schwoerer, *J. Appl. Phys.* 105 (2009) 113111.
- [40] R. Li, C. Tang, Y. Du, W. Huang, Q. Du, J. Shi, L. Yan, X. Wang, *Rev. Sci. Instrum.* 80 (2009) 083303.
- [41] S. Tokita, S. Inoue, S. Masuno, M. Hashida, S. Sakabe, *Appl. Phys. Lett.* 95 (2009) 111911.
- [42] P. Musumeci, J.T. Moody, C.M. Scoby, M.S. Gutierrez, M. Westfall, *Appl. Phys. Lett.* 97 (2010) 063502.
- [43] Y. Murooka, N. Naruse, S. Sakakihara, M. Ishimaru, J. Yang, K. Tanimura, *Appl. Phys. Lett.* 98 (2011) 251903.
- [44] P. Baum, A.H. Zewail, *Chem. Phys. Lett.* 462 (2008) 14.
- [45] M. Eichberger, N. Erasmus, K. Haupt, G. Kassier, A. von Flotow, J. Demsar, H. Schwoerer, *Appl. Phys. Lett.* 102 (2013) 121106.
- [46] A. Buck, M. Nicolai, K. Schmid, C.M.S. Sears, A. Sävert, J.M. Mikhailova, F. Krausz, M.C. Kaluza, L. Veisz, *Nat. Phys.* 7 (2011) 543.
- [47] R.P. Chatelain, V.R. Morrison, C. Godbout, B. van der Geer, M. De Loos, B.J. Siwick, *Ultramicroscopy* 116 (2012) 86.
- [48] V.A. Lobastov, R. Srinivasan, A.H. Zewail, *Proc. Natl. Acad. Sci. U.S.A.* 102 (2005) 7069.
- [49] P. Baum, A. Schild, J. Manz, *Sci. China G* 53 (2010) 987.
- [50] S. Naumov, A. Fernandez, R. Graf, P. Dombi, F. Krausz, A. Apolonski, *New J. Phys.* 7 (2005) 216.
- [51] T. Ganz, V. Pervak, A. Apolonski, P. Baum, *Opt. Lett.* 36 (2011) 1107.
- [52] C. Homann, C. Schriever, P. Baum, E. Riedle, *Opt. Express* 16 (2008) 5746.
- [53] P. Hommelhoff, Y. Sortais, A. Aghajani-Talesh, M.A. Kasevich, *Phys. Rev. Lett.* 96 (2006) 077401.
- [54] B. Barwick, C. Corder, J. Strohaber, N. Chandler-Smith, C. Uiterwaal, H. Batelaan, *New J. Phys.* 9 (2007) 142.
- [55] C. Ropers, D.R. Solli, C.P. Schulz, C. Lienau, T. Elsaesser, *Phys. Rev. Lett.* 98 (2007) 043907.
- [56] A. Paarmann, M. Gulde, M. Müller, S. Schäfer, S. Schweda, M. Maiti, C. Xu, T. Hohage, F. Schenk, C. Ropers, R. Ernstorfer, *J. Appl. Phys.* 112 (2012) 113109.
- [57] B.J. Claessens, S.B. van der Geer, G. Taban, E.J.D. Vredenburg, O.J. Luiten, *Phys. Rev. Lett.* 95 (2005) 164801.
- [58] A.J. McCulloch, D.V. Sheludko, S.D. Saliba, S.C. Bell, M. Junker, K.A. Nugent, R.E. Scholten, *Nat. Phys.* 7 (2011) 785.
- [59] C. Weninger, P. Baum, *Ultramicroscopy* 113 (2012) 145.
- [60] A. Damascelli, *Phys. Scr.* T109 (2004) 61.
- [61] K.L. Jensen, J.J. Petillo, E.J. Montgomery, Z. Pan, D.W. Feldman, P.G. O'Shea, N.A. Moody, M. Cahay, J.E. Yater, J.L. Shaw, *J. Vac. Sci. Technol. B* 26 (2008) 831.
- [62] Z. Tao, H. Zhang, P.M. Duxbury, M. Berz, Chong-Yu Ruan, *J. Appl. Phys.* 111 (2012) 044316.
- [63] W.E. Spicer, *Phys. Rev. Lett.* 11 (1969) 243.
- [64] A. Janzen, B. Krenzer, O. Heinz, P. Zhou, D. Thien, A. Hanisch, F.-J. Meyer zu Heringdorf, D. von der Linde, M. Horn von Hoegen, *Rev. Sci. Instrum.* 78 (2007) 013906.
- [65] C.T. Hebeisen, G. Sciaini, M. Harb, R. Ernstorfer, T. Dartigalongue, S.G. Kruglik, R.J.D. Miller, *Opt. Express* 16 (2008) 3334.
- [66] P. Reckenthaeler, M. Centurion, V.S. Yakovlev, M. Lezius, F. Krausz, E.E. Fill, *Phys. Rev. A* 77 (2008) 042902.
- [67] B. Barwick, D.J. Flannigan, A.H. Zewail, *Nature* 462 (2009) 902.
- [68] J.C.H. Spence, *High-Resolution Electron Microscopy*, Oxford University Press, 2003.
- [69] M. Born, E. Wolf, *Principles of Optics: Electromagnetic Theory of Propagation, Interference and Diffraction of Light*, Pergamon Press, 1970.
- [70] A.H. Zewail, J.M. Thomas, *4D Electron Microscopy: Imaging in Space and Time*, Imperial College Press, 2010.
- [71] B. Cho, T. Ichimura, R. Shimizu, C. Oshima, *Phys. Rev. Lett.* 92 (2004) 246103.
- [72] T. van Oudheusden, E.F. de Jong, S.B. van der Geer, W.P.E.M. Op't Root, O.J. Luiten, B.J. Siwick, *J. Appl. Phys.* 102 (2007) 93501.
- [73] B. McMorran, A.D. Cronin, *Phys. Rev. A* 78 (2008) 013601.
- [74] A.M. Michalik, E.Y. Sherman, J.E. Sipe, *J. Appl. Phys.* 104 (2008) 054905.
- [75] The uncertainty relation in the energy-time domain is sometimes disputed. Using the longitudinal momentum spread to derive the longitudinal extent of the wave function produces the same results.
- [76] S.A. Hilbert, C. Uiterwaal, B. Barwick, H. Batelaan, A.H. Zewail, *Proc. Natl. Acad. Sci. U.S.A.* 106 (2009) 10558.
- [77] G. Dixit, O. Vendrell, R. Santra, *Proc. Natl. Acad. Sci. U.S.A.* 109 (2012) 11636.
- [78] M. Hentschel, R. Kienberger, Ch. Spielmann, G.A. Reider, N. Milosevic, T. Brabec, P.B. Corkum, U. Heinzmann, M. Drescher, F. Krausz, *Nature* 414 (2001) 509.
- [79] A. Baltuška, T. Udem, M. Uiberacker, M. Hentschel, E. Goulielmakis, C. Gohle, R. Holzwarth, V.S. Yakovlev, A. Scrinzi, T.W. Hänsch, F. Krausz, *Nature* 421 (2003) 611.
- [80] R. Kienberger, E. Goulielmakis, M. Uiberacker, A. Baltuška, V. Yakovlev, F. Bammer, A. Scrinzi, Th. Westerwalbesloh, U. Kleineberg, U. Heinzmann, M. Drescher, F. Krausz, *Nature* 427 (2004) 817.
- [81] A.H. Zewail, *Angew. Chem. Int. Ed.* 39 (2000) 2587.
- [82] P.B. Corkum, F. Krausz, *Nat. Phys.* 3 (2007) 381.
- [83] F. Krausz, M. Ivanov, *Rev. Mod. Phys.* 81 (2009) 163.